Development of a Bionic Leg Robot for Knee Exoskeleton Test

Chien-Wu Lan, *Member, RST*, Bo-Sian Chen, Chi-Ting Ku, Ming-Fang Lo, and Kuo-Kuang Jen

***Abstract*—With the increase of exoskeleton products, how to provide standard measurement and objective evaluation of exoskeleton becomes important. However, the instability and cumbersome procedures of traditional body-worn test methods make them difficult. In this research, a bionic leg robot suitable for knee exoskeleton testing is proposed. By executing repeatable designed test actions, the bionic leg test platform can provide stable test conditions and achieves a reliable exoskeleton experimental environment. In addition, the test platform can provide angles, angular velocities, and load currents trajectories of each joint of the bionic legs during executing actions. This information can be further used as characteristic analysis for an exoskeleton. For more, the outline of the bionic legs is composed of detachable parts made by 3D printing, so desired leg shape can be customized according to the needs of exoskeleton test conditions. Finally, designed test action was performed on the bionic leg test platform wearing a knee exoskeleton, and measured data are analyzed to verify the feasibility and effectiveness of the test platform proposed in this research.**

***Index Terms*—bionic leg, exoskeleton, motion analysis, system integration, test platform**

I. Introduction

Due to the improvement of exoskeleton-related technologies in recent years, exoskeleton products for normal people assistance have gradually increased. At the same time, how to effectively evaluate the performance of the exoskeleton has also become a rather challenging topic. Generally, the popular method for exoskeleton verification is to wear an exoskeleton on a tester to perform several planned exercises, such as jogging or running for a few minutes on a Treadmill. Then various sensors are used to measure and record the movement trajectories and physiological information, such as body temperature and blood oxygen concentration of the tester at the same time. The recorded data are used to determine whether the tester's physical state has improved or not after wearing the exoskeleton, to indirectly evaluate the performance of the worn exoskeleton. For instance, Kirby et al. measured various physiological values of runners who are wearing a motorized ankle exoskeleton and running on a treadmill; and put forward the evaluation conclusion that their proposed exoskeleton can improve runners' speed by 10% [1]. Ding et al. used the Vicon T series camera system for motion capture and recorded of wearer's movement trajectory, and used Bertec treadmills to measure the ground reaction force (GRF) of the wearer [2]. Then they used the recorded data to analyze the gait dynamics. They also measured the wearer's surface electromyography (sEMG) to evaluate the wearer's muscle metabolism. The analysis result is used to prove the impact of their designed soft exoskeleton on the wearer's behavior and determine the exoskeleton's efficacy.

However, because human behavior is a highly time-varying system, for example, even a regular walking action, there will still be slight differences between the previous step and the next step, and the physiological state is also varying with time. Therefore, to evaluate exoskeleton performance according to human beings' information is unreliable, and endurance testing also cannot be performed on wearer for a long time. Moreover, each tester has a different height, weight, and body shape, so it is difficult to aggregate several individual assessments into a common standard. For more, relying on a tester to evaluate the efficacy of the exoskeleton may not only delay the development process, but may also pose an injury risk to the tester. Therefore, several researchers have begun to develop an automated measurement system for exoskeletons, such as the exoskeleton test gantry platform system developed by the Rotary Machinery and Dynamics Control Laboratory of Cleveland State University [3], which includes a treadmill that can provide a long-term walking test as an early evaluation of exoskeleton. The Human Dynamics and Control Laboratory of the University of Illinois Urbana-Champaign has also developed a pneumatic test platform for upper limb exoskeleton testing [4]. The test platform is modeled according to published anthropometric data for a 50th percentile American male, which can perform reliable, repeatable, and safe experiments on different exoskeletons without volunteers. And the measurement process is fast and without affecting by human factors.

In order to develop a test platform suitable for evaluating the performance of knee exoskeletons, performance analysis techniques of various exoskeleton research are discussed. Firstly, several searches evaluate exoskeleton characteristics through torque measurement [5-10]. Zhang et al. developed a soft knee exoskeleton driven by a vacuum-driven rotary actuator [5]. The internal air pressure, rotation angle, and output force of the actuator are used to construct a knee torque model. The knee torque model then is combined with a gait estimation model to calculate the performance of an exoskeleton. And the metabolic cost of walking reduced by 6.85% was claimed when wearing the proposed exoskeleton. Xu et al. proposed an auxiliary torque control strategy for a bionic knee exoskeleton based on real-time

The authors deeply acknowledge finance support from the National Chung-Shan Institute of Science and Technology of Taiwan with Grant number: NCSIST-502-V304 (111).

C. W. Lan is with the Department of Electrical and Electronic Engineering, Chung Cheng Institute of Technology, National Defense University, Taoyuan City 335, Taiwan (e-mail: chienwulan@gmail.com).

B. S. Chen is with the Department of Electrical and Electronic Engineering, Chung Cheng Institute of Technology, National Defense University, Taoyuan City 335, Taiwan (e-mail: kid19910621@gmail.com).

C. T. Ku is with the Department of Electrical and Electronic Engineering, Chung Cheng Institute of Technology, National Defense University, Taoyuan City 335, Taiwan (e-mail: bj42822404@gmail.com).

Ming-Fang Lo is with the Missile and Rocket Research Division, National Chung-Shan Institute of Science & Technology, Taoyuan City 325, Taiwan (e-mail: luo@ncsist.org.tw).

Kuo-Kuang Jen is with the Missile and Rocket Research Division, National Chung-Shan Institute of Science & Technology, Taoyuan City 325, Taiwan (e-mail: JKK@ncsist.org.tw).

gait event detection [6-7]. The control model is trained by collecting data on walking with the exoskeleton in zero torque mode and assisted torque control mode, respectively. And the real-time experiments are carried out by 5 subjects to verify the effectiveness of the exoskeleton control algorithm. Lee et al. also made experiments on 12 subjects walking uphill and downhill with and without auxiliary output of exoskeleton, and measured torque and physiological metabolism information of subjects [8]. The measured torque was used to calculate mechanical energy. Then the calculated energy and physiological metabolism information were used to assess the efficacy of exoskeletons. Sarkisian et al. proposed an exoskeleton with a prismatic revolute-revolute (PRR) self-aligning structure [9], and also measured the torque of an exoskeleton to determine whether the energy output by the exoskeleton could be delivered to the wearer. Park et al. also used the measured torque to estimate the energy of a developed exoskeleton, and then evaluated the auxiliary performance of the exoskeleton in the scenario of 6 subjects walking 10 degrees up and down a slope [10].

On the other hand, in addition to analyzing the performance of exoskeletons by torque energy, some researchers focus on analyzing the relationship between human behavior and exoskeleton behavior prediction [11-20]. Cardona et al. established a complete model of human muscle and skeleton, and then evaluated the reference trajectory for exoskeleton-assisted movement under various action modes and walking stages of wearers [11]. Auberger et al. also analyzed walking track intervals of 5 motion modes, such as up and down stairs, slope, and plane to assess the performance of a developed exoskeleton [12]. Martínez et al. designed a multi-joint control method based on a flow controller to create motions of a lower limb exoskeleton driven by a single joint, and defined its ideal trajectory [13]. The control method was tested on 3 subjects, and verified the auxiliary effect by subjective feedback. Li et al. evaluated the performance characteristics of a developed reducer-driven lower limb exoskeleton by analyzing angles, velocity, and current values returned by the actuator and the target trajectory of the exoskeleton [14]. Zhong et al. also judged whether an exoskeleton can correctly assist a wearer's movements by comparing the difference between real angular trajectories of an actuator of the exoskeleton and a target trajectory generated by a proposed algorithm [15-17]. Chen et al. converted the center of mass trajectories of a tester in walking posture into an offline running trajectory for exoskeleton through inverse kinematics. The offline trajectory can be modified online as a target trajectory for real-time control of the exoskeleton [18-20]. Then a real-time center of mass trajectory was calculated by measuring pressure sensors and compared with the target trajectory. The compared result judged whether the exoskeleton recognizes the tester's behavior and assists correctly.

Based on the results of the aforementioned research, the torque load and the trajectory of an exoskeleton are suitable for analyzing the performance of the exoskeleton. Therefore, in this research, we propose a bionic leg test platform [21-24], which can provide actuators' loading current, moving speed, and motion trajectory information. The information can be used to evaluate an assistant state while wearing an exoskeleton on the bionic leg. How to implement the test platform is introduced in Section II of this paper. In section III, a test motion pattern design and test scenario for the test platform are explained. Results of experiments and discussion are presented in section IV, and made conclusions in section V.

II. System Implementation

To explain how to realize the developed test platform, in this paper, the implementation of the test platform is divided into three parts: system architecture, software framework, and bionic leg fabrication. Details of these parts are described below.

A. System Architecture

The test platform has three main components: bionic legs, control and data acquisition system, and user interface, as shown in Fig. 1. Since most knee exoskeletons only have one degree of freedom (DOF) in a single support joint, the bionic leg is designed to have only four DOFs: the left hip, right hip, left knee, and right knee. The design can not only reduce too many influence factors from complex motions of the bionic leg, but also form a one-to-one correspondence between the driving axis of the bionic leg and the auxiliary axis of the exoskeleton, and can make subsequent testing and analysis more concise. The detail of bionic fabrication is described in subsection B. In addition, to avoid the influence of the balance control of the bionic legs operating on the ground to affect the test and analysis of an exoskeleton, a hanger was designed to suspend the bionic legs for experiments.

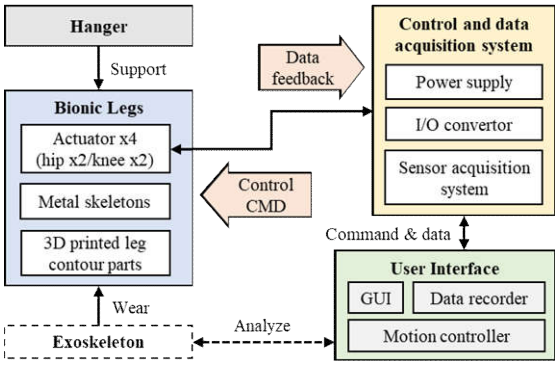

Fig. 1. System architecture of the test platform.

On the other hand, motions of the bionic leg are generated by the user interface. The interface has a graphical user interface (GUI), through which users can send control commands to operate the bionic leg to execute designed actions. In addition, data measured by sensors on the bionic leg will also be sent back to the user interface while actions are being performed by the bionic legs. These data can be recorded through the user interface for subsequent analysis of an assistive performance of an exoskeleton.

Finally, the control and data acquisition system shoulders the functions of command transmission, sensing data feedback, and data signal and format conversion between the bionic leg and the user interface. In addition, the power of bionic legs is also supplied by the control and data acquisition system.

B. Bionic Leg Implementation

The skeleton of bionic legs is made of metal frames. For the connection between the metal frames, Robotis PH54-200-S500-R servos are used as the connection joints. Additionally, the servos can feedback angular position, angular speed, and load currents information, which can be used as

motion trajectories of the bionic legs and provide for exoskeleton analysis. The assembled skeleton of the bionic leg is installed on a waist structure, which is made of aluminum extrusion, and then suspended on the hanger through the waist structure. As for contours of the bionic legs, 3D printed parts are used to make them, which can be customized according to leg shapes that need to be tested in the exoskeleton. Several printed contour parts design of the bionic leg is shown in Fig. 2(a). In addition, mounting holes are designed on the metal frames, which can provide 3D printed leg contour parts for installation and adjustment. The front and back views of the bionic legs which have been mounted with the 3D printed leg contour parts on its skeleton are depicted in Fig. 2(b). The developed test platform is about 0.34 m wide at its waist, about 0.41 m long from its hip joint to its knee joint, and also about 0.41 m long from its knee joint to its leg end (ankle), and weighs at each bionic leg is about 8.7 kg, which will vary for different 3D printed parts. The specification of bionic legs is listed in Table I.

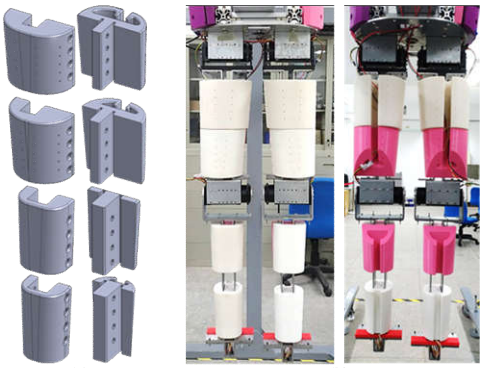

(a) (b)

Fig. 2. (a) Printed contour parts design and (b) the front and back view of the bionic legs.

TABLE I
SPECIFICATION OF THE BIONIC LEGS

Parts	Left Leg	Right Leg
Hip joint weight (servo with hinge parts)	1.0 kg	1.0 kg
Knee joint weight (servo with hinge parts)	1.0 kg	1.0 kg
3D printed parts weight	1.9 kg	1.9 kg
Skeletons weight	4.8 kg	4.8 kg
Thigh Length	0.41 m	0.41 m
Calf length	0.41 m	0.41 m

C. *Software Framework*

In terms of the software framework of the user interface, C# language is used in this research to develop the GUI required for manipulating the bionic legs and recording its experimental sensing data. Besides, the function library of .Net Framework 4 is used for GUI development, which makes the GUI compatible with Windows 10 64-bit operating system version. Besides, after separating an action designed to perform on the bionic legs into a plurality of key frames, angles and rotation speeds of each joint in each key frame of the action can be established in the form of an array table. Then the array table can be established in the user interface. Based on the application programming interface (API) provided by Robotis dynamixel software development tool (SDK), users can convert angle and rotation speed in the array table of a key frame into servo control commands, and then control the bionic legs to execute desired actions through the GUI. The I/O signal conversion between the servos and the user interface can be converted through the serial port transmission API (COM library). Finally, the angular position, rotation speed, and load currents of a servo measured in real time during operation can also be sent back to the user interface through the API of the Robotis dynamixel SDK and the COM library for recording. And then users can observe and edit the recorded data through the GUI for exoskeleton analysis. The complete software operation framework of this study is shown in Fig. 3.

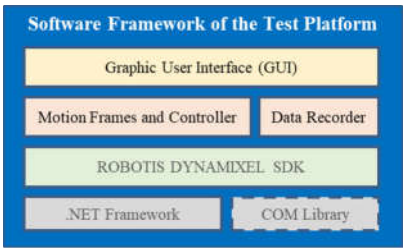

Fig. 3. Software framework of the test platform.

III. EXPERIMENT DESIGN AND PLANNING

To understand data presentation form of the test platform for the load state of the bionic legs, we first analyze the relationship between the load state of the bionic legs and the feedback currents of the servo in the bionic leg. Next, in order to design actions that can be applied to an exoskeleton wearing test on bionic legs, motion trajectories performed by a human body are recorded and provided as a test action to the bionic leg for execution. Details of the aforementioned experimental design are described below.

A. *Servo Load Test*

Since the servos used in this research can only feedback load currents but not torque, we connect the servo and different weights through a metal rod in order to establish the relationship between the load currents and the torque of a servo, as shown in Fig. 4(a). When the servo rotates, the connected weight will also be driven by the metal rod to rotate, and different load currents will be measured from different rotation degrees and weights. Therefore, by establishing a physical model of the experimental system, the relationship between load currents and torque of the servo can be known.

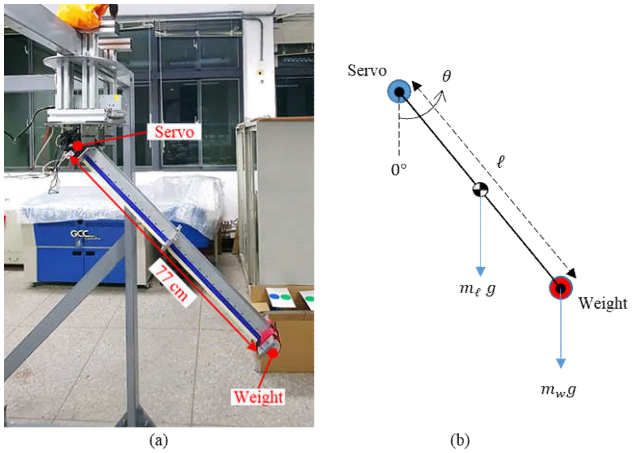

(a) (b)

Fig. 4. (a) Servo load test scenario and (b) its physical model

Assuming that the rotation angle of the servo is θ, the length of the metal rod is ℓ, the mass of the metal rod and the weight are m_ℓ and m_w, respectively, and the acceleration of gravity is *g*, as shown in Fig. 4(b), then the kinetic energies and potential energies of the metal rod and the weight can be represented by equations (1) and (2), in which k_ℓ and k_w are kinetic energies, p_ℓ and p_w are potential energies of the metal rod and the weight, respectively. In addition, $\dot{\theta}$ is the rotation velocity of the servo. Subscripts ℓ and *w* denote the quantity associated with the mental rod and the weights.

$$k_\ell = \frac{1}{6} m_\ell \ell^2 \dot{\theta}^2 ,\ k_w = \frac{1}{2} m_w \ell^2 \dot{\theta}^2 \tag{1}$$

$$p_\ell = -\frac{1}{2} m_\ell g \ell \cos\theta ,\ p_w = -m_w g \ell \cos\theta \tag{2}$$

According to the Lagrangian mechanics theorem, the torque or force of the system can be obtained by differentiating the energy in the system with respect to system variables and time [25]. Lagrangian of the previous system can be calculated by the formula (3), and torque of the servo can be calculated by the formula (4), where $\ddot{\theta}$, b_s and f_s are angular acceleration of the servo, viscous friction coefficient, and Coulomb friction, respectively [26-27]. Subscript *s* denotes the quantity associated with the servo.

$$\begin{aligned} L &= k_\ell + k_w - p_\ell - p_w \\ &= \left(\frac{1}{6} m_\ell + \frac{1}{2} m_w\right) \ell^2 \dot{\theta}^2 + \left(\frac{1}{2} m_\ell + m_w\right) g \ell \cos\theta \end{aligned} \tag{3}$$

$$\begin{aligned} \tau_s &= \frac{\partial}{\partial t}\left(\frac{\partial L}{\partial \dot{\theta}}\right) - \frac{\partial L}{\partial \theta} \\ &= \left(\frac{1}{3} m_\ell + m_w\right) \ell^2 \ddot{\theta} + \left(\frac{1}{2} m_\ell + m_w\right) g \ell \sin\theta + b_s \dot{\theta} + f_s sign(\dot{\theta}) \end{aligned} \tag{4}$$

Therefore, according to the above physical model, when the servo rotation experiment is carried out under conditions of known metal rod length and the weight of the metal rod and weights, the relationship between measured currents of the servo and torque values of the physical model can be established. Relevant experimental data and results are described in section IV.

B. Test Action Design

Since the bionic legs have only 4 DOFs, in order to design suitable test actions that can be performed on the bionic leg test platform, we recorded angular trajectories of hip and knee joints of both legs in the sagittal plane form subjects as test actions. In this paper, we choose experimental results of walking action as a demonstration and illustration example for the feasibility of the platform.

When moving trajectories of a subject's hip and knee joints have been recorded, these trajectories then need to be converted into control commands that can be executed by servo motors on the bionic legs. However, because the results of a motion trajectory sampling are usually composed of a large number of position points, if all these points are converted into control commands and sent to servo motors, too frequent command sending will cause the servo motors to fail to parse the commands, which will result in delays or occur errors of the test platform.

Therefore, we sample points with larger position change curvature of recorded trajectories as feature points of the trajectory, and define these feature points as key frames of a test action represented by the recorded trajectories [24]. According to the key frame sampling method, trajectories of walking test action in this research were transformed into 17 key frames. Angular positions of each joint at each key frame are listed in Table II. When the bionic leg is standing perpendicular to the ground, the angle of each joint is defined as 0°. When the rotation direction of the servos moves the bionic leg forward, the rotation angle is defined as a positive value. Conversely, if the rotation angle of the servos causes the bionic leg to move backward, the angle is defined as a negative value. Fig. 5 shows the result obtained by executing the key frame in Table II on the bionic leg platform wearing an exoskeleton. The experiment was executed under the following conditions: angular acceleration of 100 deg/sec^2 of each joint, and maximum rotation speed of 13.8 deg/sec, 81.0 deg/sec, 17.4 deg/sec, and 66.0 deg/sec of the left hip joint, left knee joint, right hip joint, and right knee joint, respectively.

TABLE II
JOINTS' POSITION IN EACH KEY FRAME OF THE WALKING TEST ACTION

Frame	Left Hip	Left knee	Right Hip	Right Knee
1	-5.6°	-2.7°	21.7°	-57.0°
2	-7.1°	-3.2°	32.3°	-36.7°
3	-9.1°	-3.2°	28.8°	-21.1°
4	14.7°	-70.0°	6.0°	-15.0°
5	27.3°	-25.0°	-0.4°	-14.8°
6	0.6°	-8.7°	22.2°	-75.7°
7	-3.6°	-9.0°	34.2°	-47.7°
8	-8.6°	-9.0°	26.4°	-16.6°
9	17.6°	-69.6°	3.5°	-12.7°
10	27.3°	-38.3°	1.0°	-12.7°
11	26.8°	-32.9°	0.4°	-12.7°
12	-0.4°	-7.3°	20.9°	-78.3°
13	-3.9°	-7.2°	33.7°	-50.2°
14	-7.8°	-7.3°	25.4°	-20.9°
15	20.7°	-51.3°	5.4°	-8.9°
16	16.9°	-34.5°	5.2°	-8.9°
17	0.0°	0.0°	0.0°	0.0°

IV. EXPERIMENTS RESULTS AND DISCUSSION

According to the experimental design described in Section III, including load test and feedback current analysis of the servos and design of exoskeleton test action, this section will analyze and discuss data measured by each experimental result.

A. Servo Load Currents Measurement

Based on the experimental scenario of section III A, different experimental conditions used in the servo load test are described in Table III. The length ℓ and the weight m_ℓ of the metal rod are 0.77 m and 4.3 kg, respectively. And the weight m_w of different weights are 0.5 kg, 1.0 kg, and 2.0 kg, respectively. Since the rotation speed $\dot{\theta}$ of the servo is set to run at a constant speed of one revolution per minute (RPM) in this experiment, the value of the angular acceleration $\ddot{\theta}$ in formula (4) is set as 0 deg/sec^2 relatively.

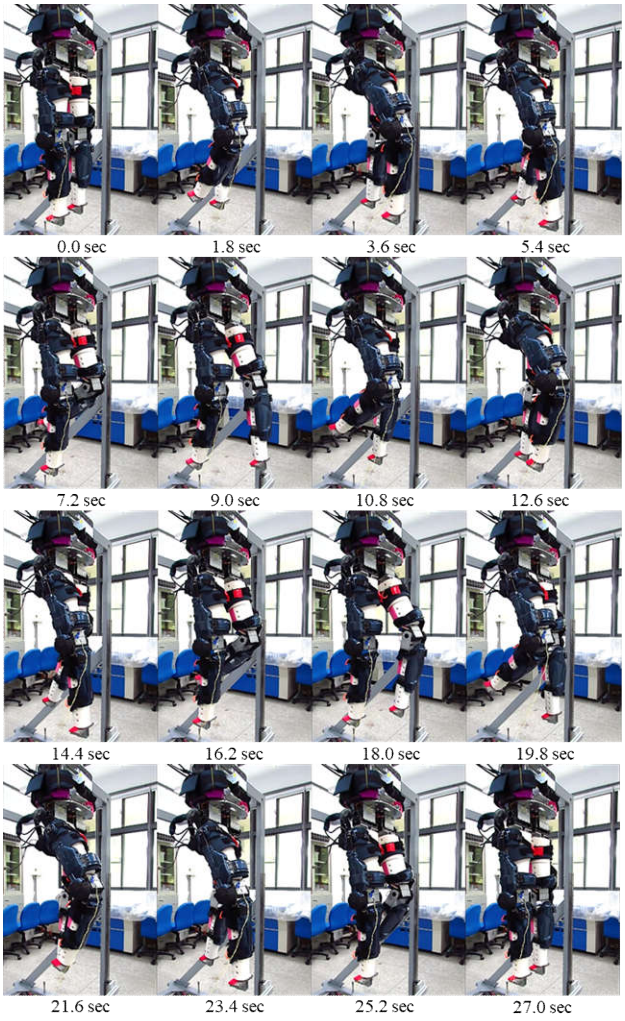

Fig. 5. Bionic leg test platform wearing exoskeleton and performing walking test action

TABLE III
EXPERIMENTAL CONDITIONS OF SERVO LOAD TEST

Length (ℓ)	Angular Velocity ($\dot{\theta}$)	Weight (m_w)	Weight (m_w)
0.77 m	1 RPM	4.3 kg	0.5 kg 1.0 kg 2.0 kg

In the experimental setup, we controlled the servo rotating from 0°to 90°, and recorded angular velocity and load currents fed back by the servo during rotation. The average data of measured results of 6 experiments under different experimental conditions are depicted in Fig. 6. Since the servo was operated by a position control mode of the load test, it can be observed from Fig. 6(a) that the average values of position trajectories measured under the experimental conditions of three different weights loads can be perfectly overlapped. However, when the rotation angle of the servo is close to 90 degrees, the influence of torque brought by gravity on the servo will gradually become obvious. In order to maintain a stable position trajectory under gradually increased gravity torque influence in the position control mode, the servo repeatedly adjusted output rotation speed, so there are obvious vibrations on speed trajectory in Fig. 6(b), and indirectly causes output current to also have obvious vibration waveforms in Fig. 6(c). This phenomenon also becomes more pronounced as the weights of the test conditions increases. On the other hand, with the increase of the weights of the test conditions, it can be observed that output currents of the servo also increase. So it can be determined that there is a corresponding proportional relationship between load currents and output torque of the servo.

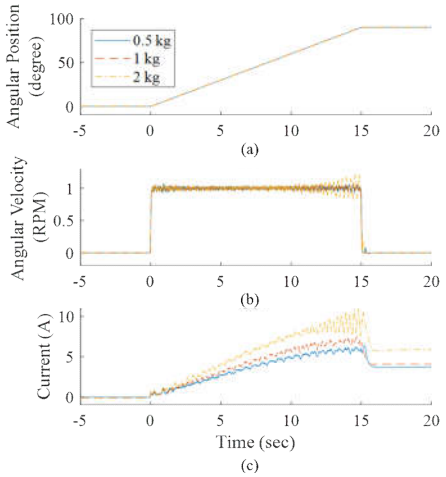

Fig. 6. (a) Angular position, (b) angular velocity, and (c) current of the servo in a load test.

In Section III, a physical model of the servo motor load test experiment has been established. Therefore, we can calculate the corresponding torque value according to recorded rotational position trajectories and angular velocity trajectories under different experimental conditions. Next, in order to find the corresponding relationship between torque and load currents of the servo, we used the curve fitting method to find the 2nd order polynomial as the relationship between torque and load currents. In addition, since the viscosity coefficient b_s and the Coulomb friction f_s of the servo are unknown, these two values are assumed to be 0 to calculate the ideal torque value under different experimental conditions. The 2nd order polynomial form of the fitted curve is described in formula (5), where τ_{sf} is torque calculated by the formula (4) in section III, i_s is measured load currents of the servos, α and β are coefficients of the first-order and quadratic terms of the formula (5), and γ is torque offset of the fitted curve.

$$\tau_{sf} = \alpha i_s^{\,2} + \beta i_s + \gamma \tag{5}$$

Based on the experimental conditions of Table III and the measured data in Fig. 6, relationships between measured current trajectories and the corresponding torque calculated by the formula (4) under different experimental conditions are depicted in Fig. 7, and their fitted curves calculated by functions of MATLAB are also depicted in Fig. 7. In order to understand the difference between fitted curves obtained from experiments and the official data [28], we also calculate the quadratic fitting curve of the relationship between current and torque from the official data of the servo, as shown in Fig. 7(a). Relationship diagrams and fitted curves of current and torque under experimental conditions of weights of 0.5 kg, 1.0 kg, and 2.0 kg are depicted in Fig. 7(b), (c), and (d), respectively.

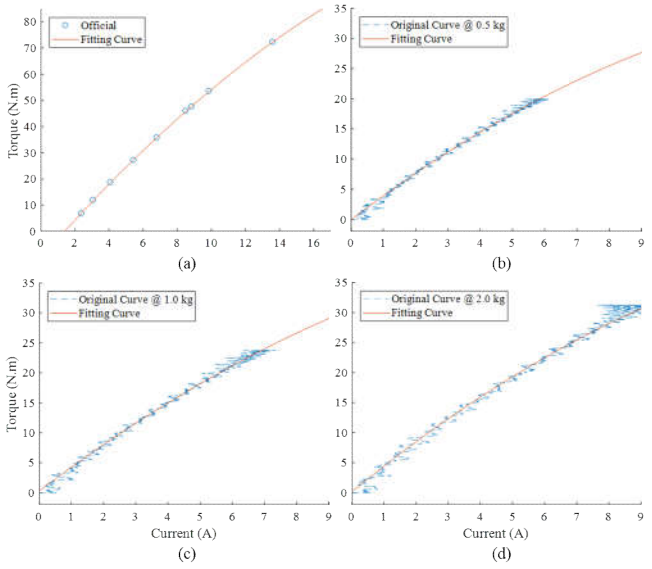

Fig. 7. Current and torque fitted curve of (a) official specification, (b) 0.5 kg, (c) 1.0 kg, and (d) 2.0 kg weights experiment results.

Calculated coefficients of formula (5) in different experimental conditions are listed in Table IV. The quadratic coefficient α of fitted curves obtained from the official specification and experimental measurement results are all about 0.1. However, there is a large difference between the coefficients of the first-order term β and the offset term γ. The difference in the first-order term coefficient β may be caused by the viscosity coefficient b_s. On the other hand, the difference in the offset term γ may be caused by the Coulomb friction f_s and individual differences among different servos. Therefore, through this servo load test, a more realistic relationship between servo load currents and borne torque in an actual environment can be found.

TABLE IV
COEFFICIENTS OF THE FITTED CURVE UNDER DIFFERENT EXPERIMENTAL CONDITIONS

Experimental Conditions	α	β	γ
Official Data	-0.10	7.46	-10.18
0.5 kg	-0.11	4.08	-0.08
1.0 kg	-0.10	4.03	-0.31
2.0 kg	-0.11	4.39	0.15

B. *Bionic Leg Test with Exoskeleton*

To verify the feasibility of the exoskeleton test on the developed test platform, we performed the test action designed in Section III B on the bionic legs with the following three scenarios: without wearing an exoskeleton, wearing an exoskeleton with auxiliary power turned off, and wearing an exoskeleton with auxiliary power turned on, respectively. The angular position, angular velocity, and load currents trajectories fed back by the test platform are shown in Fig. 8, 9, and 10, respectively. In addition, a knee exoskeleton tested in this research is provided by the National Chung Shan Institute of Science and Technology.

To provide a repeatable and stable test that cannot be provided by the human wearing method of exoskeleton test, the developed bionic leg robot is expected to have the ability to provide repeatable motion trajectories under different experimental conditions. It can be observed from Fig. 8 that under the conditions of three different test scenarios, when the bionic test platform performs the walking test action, each joint can provide similar angular position trajectories. Preliminarily meet the ability to reproduce the same motion trajectories in multi experiments.

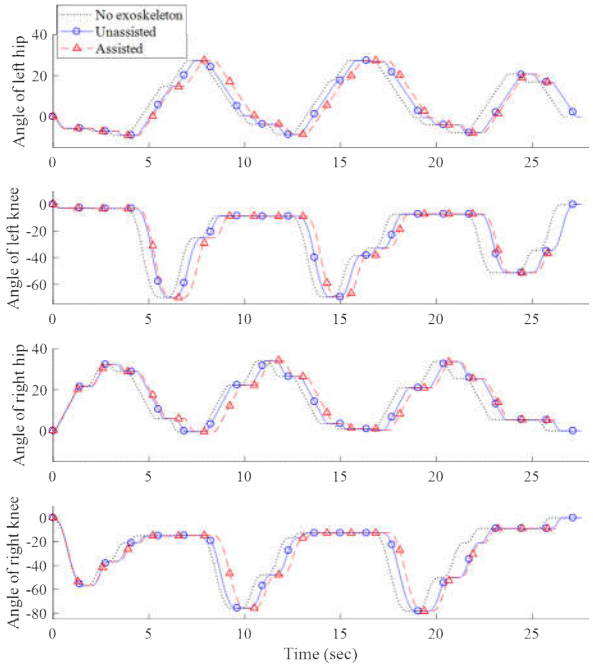

Fig. 8. Angular position trajectories of each joint of bionic legs in walking test motion under three test scenarios.

In order to make overall motion trajectories of bionic legs consistent with desired trajectories when controlling multiple servos, key frames are used as control nodes of a motion. Each Servo can't move to the position of the next key frame until all servos reach the target positions of the current key frame. On the other hand, when all servos reach the target position, angular position commands of the next key frame then can be executed synchronously on all servos.

However, from the angular position trajectories in Fig. 8, it can be found that the trajectories under different experimental scenario conditions are shifted with each other. This is caused by the difference in reaching time between each servo at a target. When each servo motor reaches a target position differently, the next target command will not be executed until the last servo reaches the target position, which also causes offset and delay between trajectories.

On the other hand, similar to the position trajectories in Fig. 8, rotation velocity trajectories in Fig. 9 are also similar to each other, and also have the phenomenon of offset from each other. Moreover, compared to the position trajectories, it can be observed that the velocity trajectories are relatively monotonic and discontinuous. This is because, in order to observe the stability of the test platform, each joint was rotated using fixed rotational speeds in this research. Furthermore, in order to achieve synchronization motion at key frames, servos will stop first when reaching target positions, and then start to rotate to the target of the next key frame. Which causes the discontinuity of velocity trajectory curves.

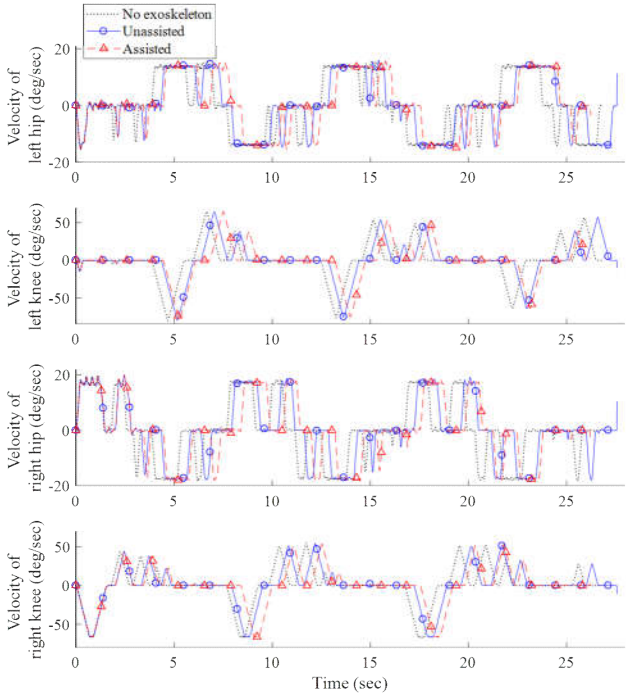

Fig. 9. Angular velocity trajectories of each joint of bionic legs in walking test motion under three test scenarios.

To present the ability of the test platform to respond to load changes of the bionic legs, we analyzed changes in load currents trajectories which are measured by the test platform under different experimental conditions. At first, to facilitate the observation of current changes under different experimental conditions, we present the current trajectories measured under three experimental conditions: before wearing the exoskeleton, and after wearing the exoskeleton with and without auxiliary power turned on. In addition, each trajectory is supplemented by a speed trajectory to understand its corresponding relationship in a motion cycle. Since the tested exoskeleton only provides auxiliary power at each knee, only the current trajectories measured by each knee of bionic legs are presented, as shown in Figures 10 and 11, respectively. Parts (a) to (c) in each figure are the trajectories measured under the three experimental conditions. From left to right are before wearing the exoskeleton, wearing the exoskeleton with, and without auxiliary power turning on.

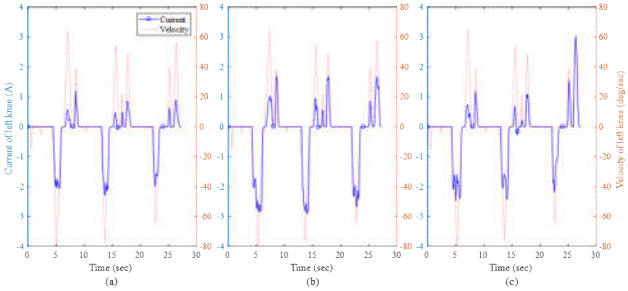

Fig. 10. Load currents with rotation velocities of the left knee under (a) before wearing the exoskeleton, (b) after wearing the exoskeleton without, and (c) with turning on the auxiliary power.

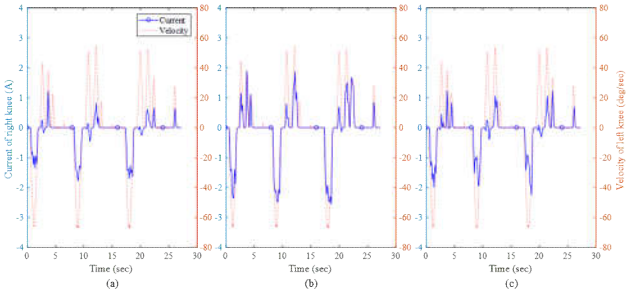

Fig. 11. Load currents with rotation velocities of the right knee under (a) before wearing the exoskeleton, (b) after wearing the exoskeleton without, and (c) with turning on the auxiliary power.

The unit of the left and right axes in each figure are currents and rotational speed, respectively. The positive and negative of the currents represent the forward and backward rotation of the knee joints. In addition, to observe currents changes only during knees' moving, we set the currents to zero when the corresponding rotation velocity is zero, and use a first-order Butterworth low-pass filter (the sampling frequency is 10 Hz, and the cut-off frequency is 2 Hz) to filter out the high-frequency noise of the current. When comparing the current trajectories in (a) and (b) of Figures 10 and 11, it can be found that the currents in part (b) of each figure increase significantly. This is because wearing an exoskeleton without turning on its auxiliary power is like wearing an extra heavy object, which causes the increasing load of the bionic legs while acting, and also causes load currents to increase. On the other hand, when wearing the exoskeleton with the auxiliary output turned on, as shown in part (c), it can be observed that the currents drop significantly compared to part (b) during the same action cycle. In addition, the current increase in the last action of Figure 11(c) may be caused by the direction of the exoskeleton assisting force being opposite to the direction of the bionic leg movement.

To identify the specific currents change under different experimental conditions, we first took the absolute value of currents; and then used the currents measured without wearing the exoskeleton as the reference to calculate the difference between currents measured under the other two experimental conditions. The calculated currents differences between different experimental conditions of the left knee and right knee are depicted in Figures 12 (a) and (b), respectively. The figure is also supplemented by rotation speed trajectories to present the corresponding relationship between currents difference and rotation speeds in motion cycles of knee joints.

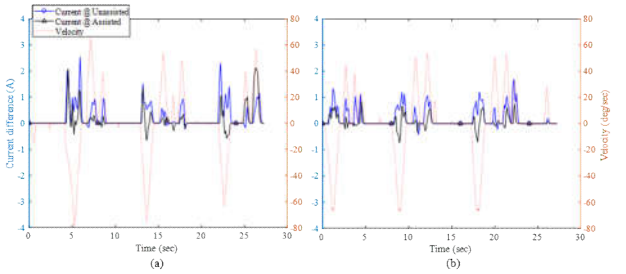

Fig. 12. Current differences between the reference and the other two experimental conditions of (a) left knee and (b) right knee.

Similar to Figures 10 and 11, the unit of the left and right axes in Figure 12 are currents difference and rotational speed, respectively. However, the positive and negative differences mean that the compared current is greater or less than the reference value. It can be observed from Figure 12 that the current measured after wearing the exoskeleton without turning on the auxiliary power is greater than the reference value, which is measured without wearing the exoskeleton, while the current measured with the auxiliary power opened exoskeleton is slightly reduced. Additionally, the latter is even smaller than the reference value in some action intervals (negative value).

Finally, the averaged current differences in Figure 12 of different experimental conditions are shown in Figure 13. The calculated results show that the current differences of the left knee measured after wearing the exoskeleton without turning on the auxiliary power, the average load current is about 0.6 A higher than that measured without wearing the exoskeleton. Relatively, currents measured after wearing the exoskeleton with turning on the auxiliary power are about 0.3 A lower than that measured without turning on the auxiliary power. In addition, the current differences between the reference and the other two experimental conditions of the right knee are 0.5 A and 0.1 A, respectively. Therefore, from Figure 13, it can be confirmed that load changes of the bionic legs can be observed by measuring load currents of the proposed test platform, and the observed load changes then can be provided for the assistance analysis of an exoskeleton indirectly.

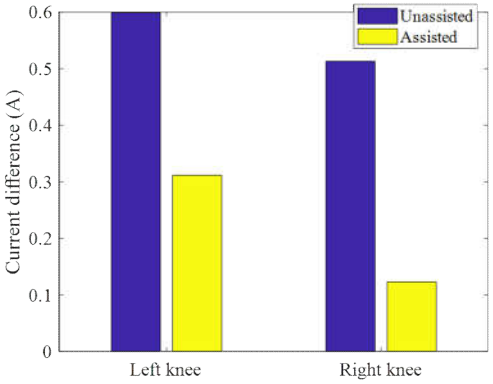

Fig. 13. The average current differences between the reference and the other two experimental conditions of (a) left knee and (b) right knee.

V. Conclusion

In this research, a bionic-legged robot test platform that can be provided for knee exoskeleton wearing and analyzing is proposed. The test platform can provide different exoskeleton wearing requirements by replacing 3D printed leg contour parts, and feedback rotation angle position, angular velocity, and load currents trajectories of joints for exoskeleton analysis. Through the servo load experiment, it is confirmed that torque change of joints of the bionic legs can be estimated by load currents fed back by servo motors. Besides, the feasibility and effectiveness of the test platform are confirmed by the experiment of wearing a knee exoskeleton on the test platform and performing the walking test action.

In addition, the developed test platform in this research expects to propose a more objective and stable novel evaluation method for exoskeleton performance measurement from the perspective of a system to a system. Therefore, the pursuit of human factors engineering and human behavior similarity is not the purpose of this study. For more, issues of trajectories offset and velocity trajectories curve discontinuity of the developed test platform can be refined in the research of control method in the future.

Finally, since the test platform is still in the development stage, test actions are designed from recorded movement trajectories from only a few subjects, which is less versatile. How to design general-purpose test actions can be discussed continually in the future.

References

[1] A. W. Kirby, F. Pieter, L. S. Alison, and H. C. Steven, "Improving the energy economy of human running with powered and unpowered ankle exoskeleton assistance," *Science Robotics*, vol. 5, no. 40, 2020. [Online]. Available: https://www.science.org/doi/10.1126/scirobotics.aay9108/

[2] Y. Ding, M. Kim, S. Kuindersma, and C. J. Walsh, "Human-in-the-loop optimization of hip assistance with a soft exosuit during walking," *Science Robotics*, vol. 3, no. 15, 2018. [Online]. Available: https://www.science.org/doi/10.1126/scirobotics.aar5438/

[3] Exoskeleton Testing Gantry Platform, facility introduction of Rotary Machinery and Dynamics Control Laboratory's webpage. [Online]. Available: https://academic.csuohio.edu/romadyc/facilities/exoskeleton-testing-gantry-platform.html/

[4] N. Thompson, A. Sinha, and G. Krishnan, "Characterizing Architectures of Soft Pneumatic Actuators for a Cable-Driven Shoulder Exoskeleton," 2019 International Conference on Robotics and Automation (ICRA), 2019, pp. 570-576.

[5] L. Zhang, Q. Huang, K. Cai, Z. Wang, W. Wang, and J. Liu, "A Wearable Soft Knee Exoskeleton Using Vacuum-Actuated Rotary Actuator," *IEEE Access*, vol. 8, pp. 61311-61326, 2020.

[6] D. Xu, X. Liu and Q. Wang, "Knee Exoskeleton Assistive Torque Control Based on Real-Time Gait Event Detection," *IEEE Transactions on Medical Robotics and Bionics*, vol. 1, no. 3, pp. 158-168, Aug. 2019.

[7] X. Liu and Q. Wang, "Real-Time Locomotion Mode Recognition and Assistive Torque Control for Unilateral Knee Exoskeleton on Different Terrains," *IEEE/ASME Transactions on Mechatronics*, vol. 25, no. 6, pp. 2722-2732, Dec. 2020.

[8] D. Lee, E. C. Kwak, B. J. McLain, I. Kang and A. J. Young, "Effects of Assistance During Early Stance Phase Using a Robotic Knee Orthosis on Energetics, Muscle Activity, and Joint Mechanics During Incline and Decline Walking," *IEEE Transactions on Neural Systems and Rehabilitation Engineering*, vol. 28, no. 4, pp. 914-923, April 2020.

[9] S. V. Sarkisian, M. K. Ishmael, G. R. Hunt, and T. Lenzi, "Design, Development, and Validation of a Self-Aligning Mechanism for High-Torque Powered Knee Exoskeletons," *IEEE Transactions on Medical Robotics and Bionics*, vol. 2, no. 2, pp. 248-259, May 2020.

[10] E. J. Park et al., "A Hinge-Free, Non-Restrictive, Lightweight Tethered Exosuit for Knee Extension Assistance During Walking," *IEEE Transactions on Medical Robotics and Bionics*, vol. 2, no. 2, pp. 165-175, May 2020.

[11] M. Cardona and C. E. García Cena, "Biomechanical Analysis of the Lower Limb: A Full-Body Musculoskeletal Model for Muscle-Driven Simulation," *IEEE Access*, vol. 7, pp. 92709-92723, 2019.

[12] R. Auberger, M. F. Russold, R. Riener, and H. Dietl, "Patient Motion Using a Computerized Leg Brace in Everyday Locomotion Tasks," *IEEE Transactions on Medical Robotics and Bionics*, vol. 1, no. 2, pp. 106-114, May 2019.

[13] A. Martínez, C. Durrough, and M. Goldfarb, "A Single-Joint Implementation of Flow Control: Knee Joint Walking Assistance for Individuals With Mobility Impairment," *IEEE Transactions on Neural Systems and Rehabilitation Engineering*, vol. 28, no. 4, pp. 934-942, April 2020.

[14] Y. Li et al., "Design and Preliminary Validation of a Lower Limb Exoskeleton With Compact and Modular Actuation," *IEEE Access*, vol. 8, pp. 66338-66352, 2020.
[15] B. Zhong, J. Cao, A. McDaid, S. Q. Xie, and M. Zhang, "Synchronous Position and Compliance Regulation on a Bi-Joint Gait Exoskeleton Driven by Pneumatic Muscles," *IEEE Transactions on Automation Science and Engineering*, vol. 17, no. 4, pp. 2162-2166, Oct. 2020.
[16] C. Chen et al., "Development and Hybrid Control of an Electrically Actuated Lower Limb Exoskeleton for Motion Assistance," *IEEE Access*, vol. 7, pp. 169107-169122, 2019.
[17] C. Chen, Z. Du, L. He, J. Wang, D. Wu, and W. Dong, "Active Disturbance Rejection With Fast Terminal Sliding Mode Control for a Lower Limb Exoskeleton in Swing Phase," *IEEE Access*, vol. 7, pp. 72343-72357, 2019.
[18] B. Chen, C. Zhong, X. Zhao, H. Ma, L. Qin, and W. Liao, "Reference Joint Trajectories Generation of CUHK-EXO Exoskeleton for System Balance in Walking Assistance," *IEEE Access*, vol. 7, pp. 33809-33821, 2019.
[19] Z. Li, C. Deng, and K. Zhao, "Human-Cooperative Control of a Wearable Walking Exoskeleton for Enhancing Climbing Stair Activities," *IEEE Transactions on Industrial Electronics*, vol. 67, no. 4, pp. 3086-3095, April 2020.
[20] A. Sarmadi, C. Schumacher, A. Seyfarth, and M. A. Sharbafi, "Concerted Control of Stance and Balance Locomotor Subfunctions—Leg Force as a Conductor," *IEEE Transactions on Medical Robotics and Bionics*, vol. 1, no. 1, pp. 49-57, Feb. 2019.
[21] C. T. Ku, "Development and Characterization of a Testing Platform for the Knee Exoskeleton," M.S. thesis, Dept. Electron. Eng., Taoyuan, Taiwan, 2021.
[22] C. -W. Lan, S. -S. Lin, C. -T. Ku, B. -S. Chen, M. -F. Lo, and M. -C. Chien, "Using Biped Robot on Knee Exoskeleton for Stair Climbing Assistance Analysis," 2021 International Automatic Control Conference (CACS), 2021, pp. 1-6.
[23] C. W. Lan, S. S. Lin, C. T. Ku, B. S. Chen, M. F. Lo, and M. C. Chien, "Design and Development of a Biped Robot for a Knee Exoskeleton Analysis," 2021 International Symposium on Intelligent Signal Processing and Communication Systems (ISPACS), 2021, pp. 1-2.
[24] B. S. Chen, "Analysis and research on the application of bionic legs in active exoskeleton aided state estimation," M.S. thesis, Dept. Electron. Eng., Taoyuan, Taiwan, 2022.
[25] S. B. Niku, "Introduction to Robotics: Analysis, Control, Applications," 3rd ed., California, USA: Wiley, 2019, pp. 220-228.
[26] C. Liang, T. Hsiao, and C. -C. Hsiao, "Joint Torque Estimation of a Powered Exoskeleton Under Compliance Control Loop," 2018 International Automatic Control Conference (CACS), 2018, pp. 1-6.
[27] C. Liang and T. Hsiao, "Admittance Control of Powered Exoskeletons Based on Joint Torque Estimation," *in IEEE Access*, vol. 8, pp. 94404-94414, 2020.
[28] Specification of Robotis PH54-200-S500-R servo. [Online]. Available: https://emanual.robotis.com/docs/en/dxl/p/ph54-200-s500-r/

Chien-Wu Lan was born in Tainan, Taiwan, 1981. He received *B.S.*, *M.S.*, and *Ph.D.* degrees from the *Department of Electrical and Electronic Engineering*, and the *School of Defense Science*, *Chung Cheng Institute of Technology*, *National Defense University*, Taoyuan, Taiwan, in 2003, 2006, and 2013, respectively. Since 2013, he is an *Assistant Professor* in the *Department of Electrical and Electronic Engineering* of *Chung Cheng Institute of Technology*, *National Defense University*. His current research interests include *humanoid robots*, *computer vision*, and *remote control*.

Bo-Sian Chen was born in Kaohsiung, Taiwan, 1991. He received *B.S.* and *M.S.* degrees from the *Department of Electrical and Electronic Engineering*, *Chung Cheng Institute of Technology*, *National Defense University*, Taoyuan, Taiwan, in 2012 and 2022, respectively. Now he is a *Technical Specialist* of the *National Chung-Shan Institute of Science and Technology* and his main task is the *R&D* and *maintenance of national defense technology*.

Chi-Ting Ku grew up in Taoyuan, Taiwan, 1997. She received an *M.S.* degree from the *Department of Electrical and Electronic Engineering*, *Chung Cheng Institute of Technology*, *National Defense University*, Taoyuan, Taiwan, in 2021. Now she is an *engineer* of the *National Chung-Shan Institute of Science and Technology*. Her current research interests include *exoskeletons* and *mental 3D printing*.

Min-Fang Lo was born in Nantou, Taiwan, 1964. He received *B.S.* and *M.S.* degrees from the *Department of Aeronautics and Astronautics Engineering*, and the *School of National Cheng Kung University* (NCKU), Tainan, Taiwan, in 1986, and 1989, respectively. Since 1989, he is an *engineer* at *National Chung Shan Institute of Science and Technology*. His current research interests include *exoskeletons*, *system control*, and *simulation*.

Kuo-Kuang Jen was born in Taichung City, Taiwan, 1963, majored in *electrical and electronic engineering* and received *B.S.* degree from the *Chung Cheng Institute of Technology, NDU*, *M.S.* from the *Chung Hua University* and *Ph.D.* from the *National Central University* Taoyuan, Taiwan, in 1986, 1995, and 2008, respectively. Since 2012, he is now the *deputy general director* of *Missile and Rocket System Research Division* of *National Chung Shan Institute of Science and Technology*. His current research interests include *exoskeletons*, *laser additive manufacture*, and *energy storage system*.